Fast-electron production in laser-heated plasmas

To cite this article: K.A. Brueckner 1977 *Nucl. Fusion* **17** 1257

NUCLEAR FUSION 17 6 (1977)

FAST-ELECTRON PRODUCTION IN LASER-HEATED PLASMAS*

K.A. BRUECKNER
Department of Physics, University of California, San Diego,
La Jolla, California,
United States of America

ABSTRACT. The continuum X-ray emission from laser-heated targets gives a measure of the energy deposited in superthermal electrons and an estimate of the spectrum and the average electron energy. The validity of the analysis is, however, limited by possible non-collisional energy-loss processes in the pellet corona. If this effect is ignored, fits to experimental X-ray spectra from glass microspheres at 1.06-μm laser wavelength can be readily obtained showing 15%–48% of the absorbed energy in fast electrons.

1. INTRODUCTION

The X-ray spectrum from laser-irradiated targets typically shows a two-component distribution, with most of the radiation emitted by a plasma at about one keV, but with a conspicuous hard component emitted by fast electrons with energies much greater than thermal. The author has suggested [1, 2] that the total energy deposited in fast electrons and the electron-energy distribution can be estimated directly from the observed X-ray spectrum. This procedure has been questioned by Brysk [3] and by Henderson and Stroscio [4]. In this paper, the original derivation is developed in more detail, an error of a factor of two in the electron energy loss rate is corrected, and the limitations of the proposed technique for analyses of experiment are analysed. The author finds that quantitative results are difficult to obtain, particularly for the electron energy spectrum, a less optimistic result than in his initial analysis [1]. Applications are made to several experimental results.

2. ANALYSIS

The bremsstrahlung emitted by an electron into all solid angles by electron-ion and electron-electron collisions per unit path length is

$$\frac{d^2 \epsilon_{rad}}{dh\nu dx} = \frac{8}{3} \langle Z^2 \rangle n_i \frac{e^2}{\hbar c} \frac{e^4}{mc^2} \frac{1}{\epsilon} G_{rad} \qquad (1)$$

The factor G_{rad} is given by Sommerfeld [5]. A useful approximation to Sommerfeld's result has been given by Elwert [6]:

$$\left(G_{rad}\right)_E = \frac{x_1}{x} \frac{1 - e^{-x}}{1 - e^{-x_1}} \ln \frac{x_1 + x}{x_1 - x} \qquad (2)$$

with

$$x = \frac{2\pi Z e^2}{h\nu}, \quad x_1 = \frac{2\pi Z e^2}{h\nu_1}$$
$$\epsilon = \frac{1}{2} m v^2, \quad \epsilon_1 = \frac{1}{2} m v_1^2 = \epsilon - h\nu \qquad (3)$$

An analysis by Berger [7] shows that Elwert's result is in error by less than 10% for $E/Z^2 > 10$ eV and by less than 3% for $E/Z^2 > 30$ eV. For the laser-heated plasmas we consider, the fast electrons are of the order of 10–50 keV and Z^2 in the range of 36 to 100, so that an error of a few percent or less is made in using Elwert's result. A more significant error may arise for more energetic electrons, as may be produced by more intense laser fields or by longer laser wavelengths. In addition, sufficiently strong fields can perturb the fast-electron motion and alter the radiation and energy loss processes. These effects are, however, relatively unimportant for the experimental conditions analysed in this paper.

Equation (1) is valid only if other acceleration or collisional processes leading to radiation are absent.

* Work supported in part by the National Science Foundation (PHY 75-02690).

Anomalous scattering of electrons by ion acoustic waves produced by plasma instabilities, for example, could increase the radiation loss rate. Equation (1) must, therefore, be considered to be a lower limit for the radiation rate.

To obtain the total energy radiated by an electron, Eq. (1) must be integrated over the slowing-down history of the electron. The electrons lose energy by collision with other electrons, by radiation, and possibly by work done against time-dependent electric fields in the low-density plasma. The latter effect may be present since the kinetic energy of expansion of the corona can result in part from the collisionless interaction of the fast electrons with the ions. This is particularly true of the fast ions observed to be characteristically produced in high-power-laser irradiations. For completeness, the analysis of this paper must therefore be supplemented by study of the production and effect of electric fields in the pellet corona. (See the following paper, this issue).

The rate of energy loss for non-relativistic electrons by collisions with the plasma thermal electrons, for electron energy much greater than the average energy of the plasma electrons, is [8]

$$\left(\frac{d\,\epsilon}{dx}\right)_{coll} = -\frac{2\pi e^4}{\epsilon} n_{e,pl} \ln \Lambda_{coll} \tag{4}$$

The argument of the Coulomb logarithm is given [9] for slow electrons by

$$\Lambda_{coll} = \frac{3}{2e^3}\left(\frac{\theta^3}{\pi n_e}\right)^{1/2} \tag{5}$$

and for fast electrons by

$$\Lambda_{coll} = \frac{2p}{\hbar k_D} = \frac{2p}{\hbar}\left(\frac{\theta}{4\pi n_e e^2}\right)^{1/2} \tag{6}$$

The previous calculations by the author [1, 2] used Eq. (6).

The radiative loss of Eq. (1) is very small compared with Eq. (4) and can be ignored in determining the slowing-down history of an average electron. The electron energy loss by work against corona fields is, however, not necessarily negligible so that Eq. (4) gives only an upper limit.

Equation (4) may now be used to obtain an alternative expression for Eq. (1). The total energy radiated by the electron in slowing down is

$$\frac{d\,\epsilon_{rad}}{dh\nu} = -\frac{8}{3}\frac{e^2}{\hbar c}\frac{e^4}{mc^2}\int_{h\nu}^{\epsilon_o} \frac{1}{\epsilon} G_{rad}\frac{dx}{d\epsilon}\, d\epsilon\, \langle Z^2\rangle n_i$$

$$= \frac{4}{3\pi}\frac{e^2}{\hbar c}\frac{1}{mc^2}\int_{h\nu}^{\epsilon_o} d\epsilon \frac{G_{rad}}{\ln \Lambda_{coll}} \langle Z^2\rangle \frac{n_i}{n_{e,pl}} \tag{7}$$

Equation (7) has been used to interpret the radiation from mono-energetic electrons incident on X-ray targets. For this case, the energy loss is to bound electrons and $n_{e,pl}$ may be replaced by Zn_i. The electron binding changes the argument of the collision logarithm (ignoring relativistic corrections) to E/I, with I the average ionization energy which can be experimentally determined by measurement of the rate of energy loss. The radiative Gaunt factor is also affected by the screening of the nuclear charge by the bound electrons. This alters the logarithmic singularity in the Gaunt factor as $h\nu \to 0$ but has little effect above $h\nu = 0.1\ \epsilon_0$.

For a thick X-ray target, Eq. (7) gives

$$\epsilon_{rad} \cong \frac{4}{3\pi}\frac{e^2}{\hbar c}\frac{Z}{mc^2}\int_0^{\epsilon_o} dh\nu \int_{h\nu}^{\epsilon_o} d\epsilon \frac{G(\epsilon_o, h\nu)}{\ln \Lambda_{coll}} \tag{8}$$

The experiments on radiation efficiency show that $\epsilon_{rad}/\epsilon_0$ is approximately proportional to ϵ_0, which results from the relatively slow variation of the ratio of the two logarithmic factors in Eq. (8). If the factor $G_{rad}/\ln \Lambda_{coll}$ is replaced by an average value, Eq. (8) gives

$$\frac{\epsilon_{rad}}{\epsilon_o} = \frac{2}{3\pi}\frac{e^2}{\hbar c}\frac{\epsilon_o Z}{mc^2}\left(\frac{G_{rad}}{\ln \Lambda_{coll}}\right)_{av}$$

$$= 3.03 \times 10^{-6}\, Z\, \epsilon_o(\text{keV})\left(\frac{G_{rad}}{\ln \Lambda_{coll}}\right)_{av} \tag{9}$$

The double integral in Eq. (8) is easily evaluated, giving the average value defined in Eq. (9), for different values of ϵ_0 and of the dimensionless parameter $2\pi Ze^2/\hbar v_0$ which enters in the radiation Gaunt factor. The result is nearly independent of ϵ_0 and Z. As an example, for Z = 30, $(G_{rad}/\ln \Lambda_{coll})_{av}$ varies by less than 10% between ϵ_0 = 10 keV and ϵ_0 = 50 keV.

Using the average value at 40 keV of 0.414, we find

$$\epsilon_{rad}/\epsilon_o = 1.25 \times 10^{-6}\ Z\ \epsilon_o(\text{keV}) \qquad (10)$$

This compares very well with the experimental result [10]

$$\epsilon_{rad}/\epsilon_o = (1.5 \pm 0.3) \times 10^{-6}\ Z\ \epsilon_o(\text{keV}) \qquad (11)$$

Equation (8) therefore has extensive experimental (as well as theoretical) confirmation although, of course, under the relatively simple conditions of X-ray target irradiation. The application to laser-heated plasmas is more difficult for the reasons previously noted.

Now returning to the plasma application, the thermal-electron density may be set equal to $\langle Z\rangle n_i$ only if the fast-electron density is much less than the thermal-electron density. This condition is expected to be well satisfied in the dense plasma where most of the collisional energy loss and radiation occur. The fast-electron density may, however, be comparable to or greater than the thermal-electron density in the low-density corona, but little collisional energy loss or radiation occurs in this region. With $n_{e,pl} = \langle Z\rangle n_i$, Eq. (8) still depends weakly on the slowing-down history of the fast electrons since the degree of plasma ionization and of temperature (which enters through the collisional Coulomb logarithm) are functions of position. These effects are, however, relatively weak and are a source of error which is unimportant compared with the uncertainty resulting from other possible electron energy loss processes in the corona.

Equation (8) is the basis for further analysis of the superthermal-X-ray spectrum. The result is valid only for electron energy well above the thermal population, and useful primarily if the radiation from the fast electrons can be separated from the X-ray emission from the high-energy tail of the plasma electrons. This condition is usually satisfied for experiments at high power with one-micron radiation. Analysis of experiment at longer wavelengths has not been made by the author because of the difficulty of obtaining adequate quantitative X-ray spectral data. Equation (8) also is only valid, as discussed above, if sources of electron-energy loss other than collisional can be neglected.

For a distribution of fast electrons produced with initial energy ϵ_0, Eq. (8) gives for the total radiated energy

$$\frac{dE_{rad}}{dh\nu} = \int_{h\nu}^{\infty} \frac{d\epsilon_{rad}}{dh\nu}(\epsilon_o, h\nu)\, N(\epsilon_o)\, d\epsilon_o$$

$$= \frac{4}{3\pi}\frac{e^2}{\hbar c}\frac{1}{mc^2}\frac{\langle Z^2\rangle}{\langle Z\rangle}\int_{h\nu}^{\infty} d\epsilon_o N(\epsilon_o)\int_{h\nu}^{\epsilon_o} d\epsilon \frac{G_{rad}}{\ln \Lambda_{coll}}$$

$$= \frac{4}{3\pi}\frac{e^2}{\hbar c}\frac{1}{mc^2}\frac{\langle Z^2\rangle}{\langle Z\rangle}\int_{h\nu}^{\infty} d\epsilon \frac{G_{rad}}{\ln \Lambda_{coll}}\int_{\epsilon}^{\infty} N(\epsilon_o)\, d\epsilon_o \qquad (12)$$

To determine the number and energy of fast electrons, Eq. (12) must now be solved for $N(\epsilon_0)$, using the measured spectrum of X-ray radiation emitted by fast electrons with energy well above the bulk thermal population. Equation (12) can, of course, be inverted by introducing a number of discrete energy groups for $N(\epsilon_0)$ and determining the separate intensities by direct inversion from the experimental data. This procedure is laborious and, in principle, can lead to ambiguous results. The simple form of the observed spectra [11, 12] suggests, however, that a simple analysis is useful. As the subsequent application to experiment shows, the X-ray spectral measurements with 1.06-μm laser radiation at power densities greater than 10^{15} W·cm^{-2} can be well described with electron-energy spectra of the form

$$N(\epsilon_o) = N_o(\exp - \epsilon_o/\epsilon_f)(\epsilon_o/\epsilon_f)^n \Big/ \epsilon_f \qquad (13)$$

giving

$$\frac{dE_{rad}}{dh\nu} = \frac{4}{3\pi}\frac{e^2}{\hbar c}\frac{1}{mc^2}\frac{\langle Z^2\rangle}{\langle Z\rangle} E_{fast}\, I_n(h\nu) \qquad (14)$$

with

$$I_n(h\nu) = \frac{1}{(n+1)!}\int_{h\nu}^{\infty}\frac{d\epsilon}{\epsilon_f}\frac{G_{rad}(\epsilon, h\nu)}{\ln \Lambda_{coll}(\epsilon)}$$

$$\times \int_{\epsilon}^{\infty}(\epsilon_o/\epsilon_f)^n(\exp - \epsilon_o/\epsilon_f)\frac{d\epsilon_o}{\epsilon_f} \qquad (15)$$

$$E_{fast} = \int_0^{\infty} N(\epsilon_o)\,\epsilon_o\, d\epsilon$$

$$= N_o(n+1)!\ \epsilon_f$$

The average electron energy is $\bar{\epsilon} = (n+1)\epsilon_f$. Equation (14) can give an unambiguous result for E_{fast} only if the ratio of the experimental X-ray spectrum $dE_{rad}/dh\nu$ to $I_n(h\nu)$ is slowly varying over a significant part of the superthermal spectrum.

The integral $I_n(h\nu)$ is a function of $h\nu/\bar{\epsilon}$ and of the dimensionless parameter

$$\lambda = \frac{2\pi Z e^2}{h}\left(\frac{m}{2\epsilon_f}\right)^{1/2} = 0.733\ Z/\epsilon_f(\text{keV})^{1/2} \qquad (16)$$

which enters through the factors x and x_1 in G_{rad}. An additional dependence on $\bar{\epsilon}$ enters through the variation with energy of the collision logarithm; this effect is, however, very weak and the logarithm can be evaluated at $\epsilon = \bar{\epsilon}$ and at a plasma temperature of one keV. Figure 1 gives the variation of $I_0(h\nu)\ \ell n\ \Lambda_{coll}$ with $h\nu/\epsilon_f$ for several values of λ. Typical values of λ range from a maximum of about 3.5 for $\epsilon_f = 9$ keV and $Z = 10$ to 0.9 for $\epsilon_f = 25$ keV and $Z = 6$. The X-ray spectrum varies slowly with λ and is approximately exponential for $h\nu/\epsilon_f$ greater than one. The slope is, however, somewhat greater than the slope of the electron spectrum; as an example, for $\lambda = 2$, the average slope from $h\nu/\epsilon_f = 1$ to $h\nu/\epsilon_f = 3$ corresponds to an apparent temperature 15% less than ϵ_f.

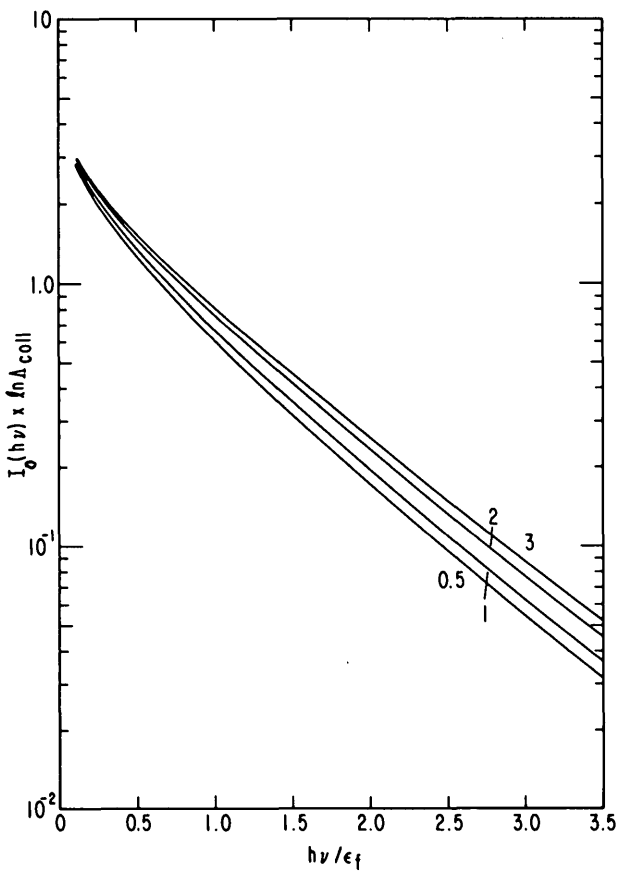

FIG.1. Computed X-ray spectra as a function of $h\nu/\epsilon_f$ and λ [see Eq. (16)], for an exponential electron distribution [n = 0; see Eq. (13)].

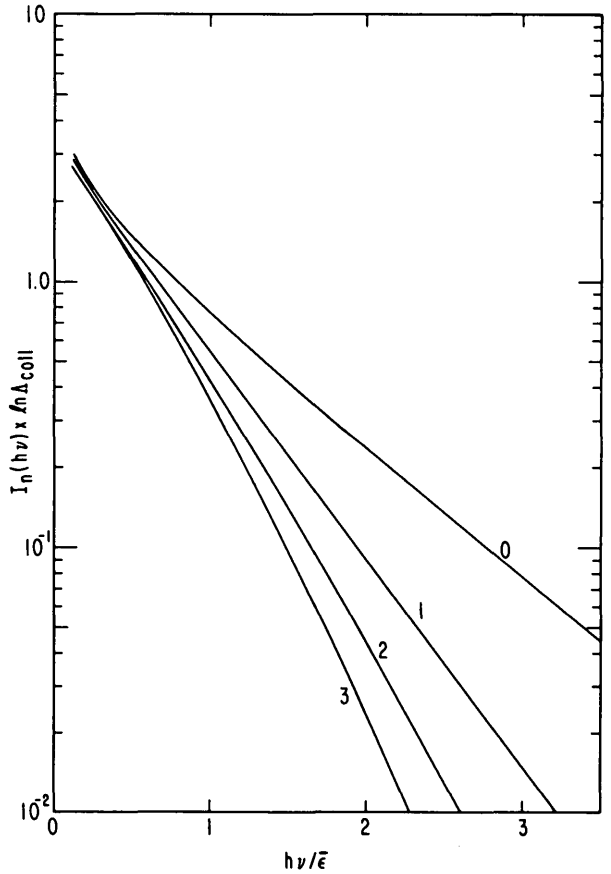

FIG.2. Computed X-ray spectra for modified electron distributions as a function of $h\nu/\bar{\epsilon}$ and n [see Eq. (13)]. The curves are labelled by n.

The shape of the computed spectra depends on the parameter n in Eq. (11). Figure 2 gives the computed spectra for $\lambda = 2$ as a function of $h\nu/\bar{\epsilon} = h\nu/(n+1)\,\epsilon_f$. The curves have approximately the same slope for $h\nu/\bar{\epsilon} \cong 1/4$ and the same projected intercept at $h\nu \to 0$ (extrapolated from $h\nu/\bar{\epsilon} > 1/2$) but have different curvature and slope for larger values of $h\nu/\bar{\epsilon}$. This behaviour is readily understood from Eq. (13). For $h\nu/\bar{\epsilon} \gtrsim 1/4$, the ratio of $G_{rad}/\ell n\ \Lambda_{coll}$ varies more slowly than the other factors in the integrand and can be replaced by an average value, giving

$$\left.\begin{aligned} \left(I_n(h\nu)\right)_{h\nu\to 0} &= \left(\frac{G_{rad}}{\ell n\ \Lambda_{coll}}\right)_{av} \\ \left(\frac{d}{dh\nu} I_n(h\nu)\right)_{h\nu\to 0} &= -\left(\frac{G_{rad}}{\ell n\ \Lambda_{coll}}\right)_{av} \frac{1}{\bar{\epsilon}} \end{aligned}\right\} \text{valid for } \frac{1}{4} \leqslant \frac{h\nu}{\bar{\epsilon}} \leqslant 1$$

For larger $h\nu/\bar{\epsilon}$, however, the slope depends on n. For fixed energy in fast electrons, the total energy radiated decreases as the electron spectrum is hardened ($n > 0$).

Again ignoring the variation of the logarithmic factors, we find

$$\int_0^\infty dh\nu\, I_n(h\nu) = \bar{\epsilon}\,\frac{n+2}{2n+2}\left(\frac{G_{rad}}{\ell n\,\Lambda_{coll}}\right)_{av} \qquad (17)$$

The following comparison with experiment shows that the energy in fast electrons can be obtained with moderate precision but that the average energy per electron, which depends on the details of the X-ray spectrum, is more difficult to determine.

To use these results in interpreting experiments, the slope of the X-ray spectrum can be read from the experimental data (assuming that an approximate fit of theory and experiment is possible), the corresponding value of $\lambda = 2\pi Ze^2/\hbar v_f$ determined, and the appropriate curve from Fig. 1 or Fig. 2 used to fit experiment. The simplest procedure is to use the extrapolation to $h\nu = 0$ from $h\nu/\bar{\epsilon} > 1/4$ of the computed and measured spectra from which Eq. (14) gives the fast electron energy directly. A more complete fit of the computed spectra to experiment can, however, give somewhat improved accuracy and a more convincing match of theory and experiment. For this purpose, inserting the appropriate constants and evaluating $\ell n\,\Lambda_{coll}$ at a plasma temperature of one keV and electron density of 10^{21} cm^{-3} and a fast-electron average energy of 15 keV, we find $\ell n\,\Lambda_{coll} = 9.30$ and

$$\frac{dE_{rad}}{dh\nu} = 4.08 \times 10^9\,\frac{\langle Z^2\rangle}{\langle Z\rangle}\,I_n(h\nu)E_{fast}(\text{joules}) \qquad (18)$$

This result depends quantitatively on the assumed electron density. If the characteristic density of thermal electrons is 10^{23} cm^{-3}, for example, as would be typical of a glass shell under some heating and compression, $\ell n\,\Lambda_{coll}$ is reduced to 7.0 and the radiated energy is increased by 33%. This source of uncertainty can be removed only if a detailed calculation of the hydrodynamic history of the implosion and of the heating processes is available and the orbiting motion of the fast electrons accurately modelled. We content ourselves in this paper with the semi-quantitative and model-independent results which can be obtained without such detailed calculation.

3. APPLICATION

Figures 3 and 4 give typical experimental results [11, 12] for glass spheres irradiated with 1.06-μm radiation. The dashed curves give the spectrum computed from Eq. (18) for n = 0 with the parameter ϵ_f determining the slope of the fast-electron distribution and the energy in fast electrons adjusted to fit the experimental result. The comparison shows that an excellent match can be easily obtained except for deviations for $h\nu/\epsilon_f$ less than unity, where the computed spectrum lies above the solid curves drawn by the experimentalists through their data. Figure 5 gives a similar comparison of theory and experiment for the electron spectrum with n = 1 [see Eq. (13)]. The computed spectrum is nearly linear with $h\nu/\bar{\epsilon}$ for $h\nu/\bar{\epsilon} > 1/4$, giving a better fit to the experimental results but requiring a considerably larger value of mean electron energy.

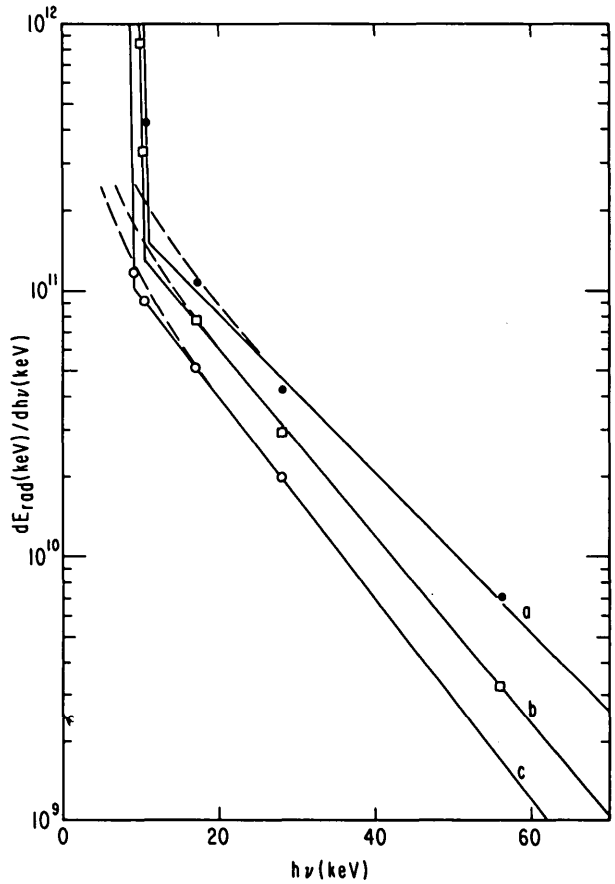

FIG.3. Experimental X-ray spectra (solid curves) and computed spectra (dashed curves). The computed and experimental spectra are essentially identical for hν greater than 30 keV. The experimental conditions are given in Table I. The solid curves are the fit by the experimentalists to the experimental results. The computed spectra are for exponential electron distributions (n = 0) and for λ = 2. The curves are labelled a, b, c corresponding to the tabulation in Tables I and II.

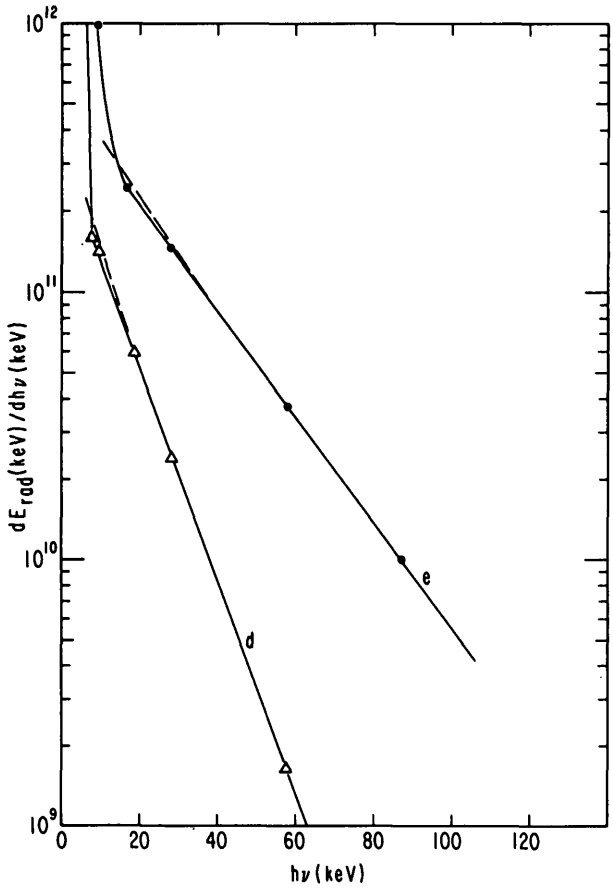

FIG.4. Same as Fig. 3, for curves d and e.

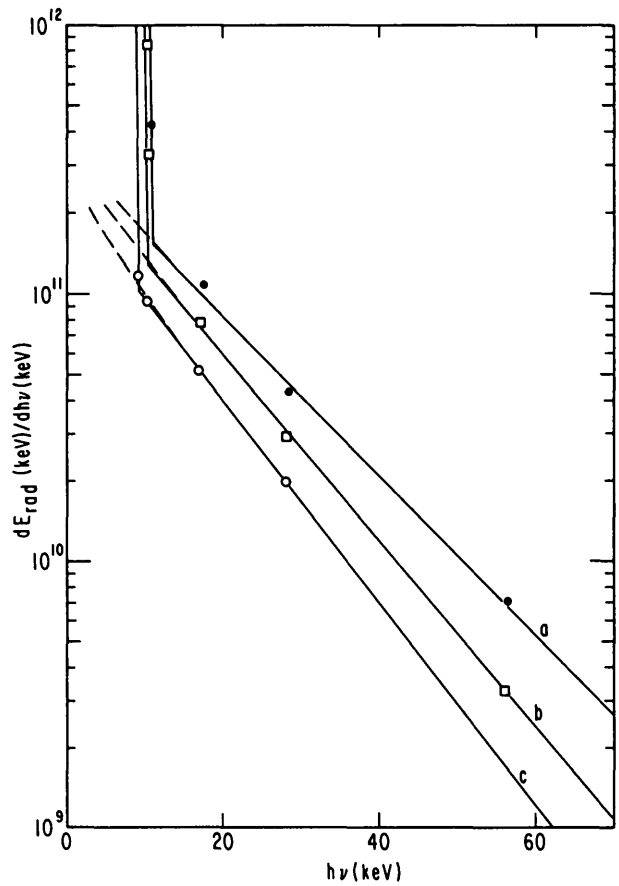

FIG.5. Comparison of theory and experiment for modified electron distributions (n = 1) and λ = 2. The experimental results are the same as in Fig. 3 and Table I. The computed and experimental spectra, as in Figs 3 and 4, are essentially identical for hν > 15 keV.

TABLE I. EXPERIMENTAL CONDITIONS AND COMPUTED FAST-ELECTRON PARAMETERS FOR EXPONENTIAL ELECTRON SPECTRA (n = 0)

	E_L (joules)	Δt (ps)	D^* (μm)	φ_L^{**} (10^{15} W·cm^{-2})	E_{abs} (joules)	ϵ_f (keV)	E_{fast} (joules)	E_{fast}/E_{abs}
a)	35.3	74	39	9.98	9.2	17	3.16	0.34
b)	30.0	71	64	3.28	8.8	14	2.96	0.34
c)	28.3	70	87	1.70	8.3	13	2.27	0.27
d)	28.3	73	86	1.67	7.4	12	3.52	0.48
e)	96.0	38	87	10.62	24.0	25	5.27	0.22

*Pellet diameter (glass microsphere)

**Average laser flux.

TABLE II. COMPUTED FAST-ELECTRON PARAMETERS FOR MODIFIED ELECTRON SPECTRA (n = 1)

	$\bar{\epsilon}$ (keV)	E_{fast} (joules)	E_{fast}/E_{abs}
a)	26	2.21	0.24
b)	21	2.07	0.24
c)	20	1.56	0.25
d)	19	2.45	0.34
e)	40	3.67	0.15

The results are summarized in Table I. The energy in fast electrons for the exponential electron spectrum (n = 0) varies from 22% to 48% of the absorbed energy with a typical value of about 30%. These results are significantly lower than the author's initial estimates [1], principally because of the previously mentioned error of a factor of two in the electron energy-loss rate. For the modified spectrum (n = 1), the average electron energy is about 60% higher and the energy in fast electrons about 30% lower. The energy in fast electrons is surprisingly low since theoretical estimates and computer simulation [13] have led to the expectation that essentially all of the absorbed energy is via resonant absorption or by other unstable processes at the critical density surface producing very energetic electrons well above the thermal population. The discrepancy can result from other absorption processes giving deposition directly into the thermal population; or, more likely, from energy loss of the fast electrons to corona electric fields which is not included in the collisional-loss process. If the latter explanation is correct, the anomalous energy loss from fast ions produced in the corona should be closely correlated with the discrepancy between the absorbed energy and the energy in fast electrons as inferred from the superthermal X-ray spectrum. (See the following paper, this issue).

4. CONCLUSION

The relatively simple interpretation of experiment given in this paper has been possible for the high-power irradiations of glass spheres with 1.06-μm radiation. Very similar results hold for glass spheres supported on disks and for CH_2 and parylene planar targets at 1.06 μm [11, 12]. The analysis for 10.6-μm radiation is more difficult, because of the much less complete experimental data and the probable marked increase in the average electron energy. Results obtained at LASL [14] at 10.6 μm show much more X-ray radiation and X-ray spectra for which the fit of the theory of this paper to experiment is more ambiguous. Alternative techniques for inversion of the X-ray spectrum to obtain the electron spectrum are, however, probably feasible, although the effect of corona fields may be more pronounced for the longer-wavelength radiation.

REFERENCES

[1] BRUECKNER, K.A., Phys. Rev. Lett. **36** (1976) 677.
[2] BRUECKNER, K.A., Phys. Rev. Lett. **37** (1976) 1247.
[3] BRYSK, H., Phys. Rev. Lett. **37** (1976) 1242.
[4] HENDERSON, D.B., STROSCIO, M.A., Phys. Rev. Lett. **37** (1976) 1244.
[5] SOMMERFELD, A., Atombau und Spektrallinien, Friedr. Vieweg & Sohn, Braunschweig, 1939, 527.
[6] ELWERT, G., Ann. Physik **34** (1939) 178.
[7] BERGER, M.J., Phys. Rev. **105** (1957) 35.
[8] BETHE, H.A., ASHKIN, J.A., Experimental Nuclear Physics, (SEGRE, E., Ed.) **1**, John Wiley & Sons, Inc., New York (1953).
[9] SPITZER, L., Jr., Physics of Fully Ionized Gases, Interscience, New York (1956).

[10] STEPHENSON, S.T., Handbuch der Physik, Springer-Verlag, Berlin **30** (1957) 337 ff.
[11] AHLSTROM, H.G., Laser-Fusion Experiments at the Lawrence Livermore Laboratory, Preprint #UCRL-77094 Rev 1, Oct. 8, 1975.
[12] STORM, E.K., AHLSTROM, H.G., BOYLE, M.J., COLEMAN, L.W., KORNBLUM, H.N., LERCHE, R.A., MacQUIGG, D.R., PHILLION, D.W., RAINER, F., RUPERT, V.C., SLIVINSKY, V.W., SPECK, D.R., TIRSELL, K.G., Laser-Fusion Experiments at 2 TW, Preprint #UCRL-78581 Rev 1, Oct. 1, 1976; Bull. Am. Phys. Soc. **21** (1973) 1173.
[13] See, e.g. FREIDBERG, J.P., MITCHELL, R.W., MORSE, R.L., RUDSINSKI, L.I., Phys. Rev. Lett. **28** (1972) 795.
[14] KEPHART, J.F., GODWIN, R.P., McCALL, G.H., Appl. Phys. Lett. **25** (1974) 108.

(Manuscript received 25 January 1977
Final version received 13 June 1977)